30 November 2001

Chemical Physics Letters 349 (2001) 257–265

CHEMICAL PHYSICS LETTERS

www.elsevier.com/locate/cplett

Competitive channels in the jet-cooled photodissociation of the CH_2Cl radical

A.B. Potter, V. Dribinski, A.V. Demyanenko, H. Reisler *

Department of Chemistry, University of Southern California, SSC 619, Los Angeles, CA 90089-0482, USA

Received 17 August 2001; in final form 22 September 2001

Abstract

The photodissociation of CH_2Cl is studied by the ion imaging technique. At 235–243 nm, Cl photofragments are produced via the simultaneous excitation of the perpendicular ($1^2A_1 \leftarrow 1^2B_1$) and parallel ($2^2B_1 \leftarrow 1^2B_1$) electronic transitions. The relative populations and translational energy distributions of Cl fragments generated via each transition are extracted. H-atom products, which are detected in a one-color experiment at 243.1 nm, exhibit an angular distribution characteristic of perpendicular transitions only. They may be produced via excitation to the valence 1^2A_1 and/or Rydberg $2^2A_1(3s)$ states.

1. Introduction

The photodissociation dynamics of methyl and halogen substituted methyl radicals is a subject of current interest, because of the role halomethyl radicals play in upper atmospheric chemistry and ozone depletion. Despite this interest, to date only the photodissociation of the methyl radical has been studied experimentally [1], and $H + CH_2(\tilde{a}^1A_1)$ has been identified as a major channel in dissociation from the lowest excited, 3s Rydberg, state.

Recently, we identified $Cl + CH_2$ as a major channel in the photolysis of CH_2Cl radicals in a molecular beam at 312–214 nm. Based on the measured product speed and angular distributions [2], and recent high-level ab initio calculations of the vertical excitation energies of CH_2Cl [3], we attributed the Cl product at $\lambda_{phot} \geqslant 247$ nm to excitation of the perpendicular $1^2A_1 \leftarrow 1^2B_1$ transition, whose vertical maximum is at ~252 nm, and identified the main dissociation channel at these wavelengths as $CH_2(\tilde{X}^3B_1) + Cl(^2P_{3/2})$. At shorter wavelengths, ca. $\lambda_{phot} \leqslant 220$ nm, the strong, parallel transition $2^2B_1 \leftarrow 1^2B_1$ dominated, and the major product channels were $CH_2(\tilde{a}^1A_1) + Cl(^2P_{1/2,3/2})$. The latter transition was also recorded in 300 K absorption, where an intense maximum around 200 nm was observed [4]. Both absorption bands are continuous, indicating fast dissociation. The dominance of the Cl channel is expected based on the antibonding nature of the orbitals involved in the excitation (see Section 4) [3].

In the region $235 \leqslant \lambda_{phot} \leqslant 243$ nm, the angular distributions of the $Cl(^2P_{1/2,3/2})$ products are speed dependent, and the effective recoil anisotropy pa-

* Corresponding author. Fax: +1-213-746-4945.
E-mail address: reisler@chem1.usc.edu (H. Reisler).

0009-2614/01/$ - see front matter
PII: S0009-2614(01)01175-7

rameter, β_{eff}, changes from positive to negative as the product speed increases. This indicates that parallel and perpendicular transitions are excited simultaneously, and that the Cl product translational energy distributions arising from these transitions are different.

In this Letter, we focus on the wavelength region in which simultaneous optical excitation to more than one excited state is observed. From the measured β parameters in spectral regions where a single electronic transition dominates and the variation of β_{eff} with Cl speed, we are able to extract the fraction of Cl products that is generated via each of the excited states, and determine its corresponding translational energy distribution.

We also report the first observation of H-photofragments (obtained by one-color photodissociation/detection at 243.1 nm), and describe their translational and angular distributions. Our interest in the H + CHCl channel derives from the proximity of its thermochemical threshold to that of the $Cl + CH_2$ channel [2]:

$$CH_2Cl \rightarrow Cl + CH_2 \quad \Delta H = 391 \pm 5 \text{ kJ mol}^{-1} \qquad \text{(I)}$$

$$CH_2Cl \rightarrow H + CHCl \quad \Delta H = 395 \pm 5 \text{ kJ mol}^{-1} \qquad \text{(II)}$$

Based on the similarity between the H-atom translational energy and angular distributions obtained in the photodissociation of CH_3 and CH_2Cl, we raise the possibility that the perpendicular transition to the Rydberg 3s state also contributes to channel II.

2. Experimental methods

2.1. Radical production

CH_2Cl radicals are produced by thermal decomposition of chloroiodomethane (CH_2ClI) in a pulsed pyrolysis source, as described before [2]. According to known thermochemical data [5–12], the lowest energy dissociation channel of CH_2ClI leads to $CH_2Cl + I$ ($\Delta H^\circ = 242$ kJ/mol). The next two channels, $CHCl + HI$ and $CH_2I + Cl$, have higher thermochemical thresholds: $\Delta H^\circ = 337$ and 367 kJ/mol, respectively. This difference allows optimization of the conditions in the pulsed pyrolysis source to maximize production of CH_2Cl.

The experiments are performed using a pulsed molecular beam containing 1.0% CH_2ClI in 1.0 atm of He. The gas mixture is prepared by passing the carrier gas over CH_2ClI (Fluka, $\geqslant 97\%$ purity) kept at −18 °C in a benzyl alcohol slush. The mixture is expanded through a pulsed piezoelectric valve (10 Hz repetition rate) with a heated SiC tube nozzle [13]. The optimal conditions of the pulsed pyrolysis source are determined by measuring the relative yields of CH_2Cl and HI in the molecular beam with 2 + 1 REMPI at 303.18 nm or 300.1 nm, respectively [2,14], at several nozzle temperatures and backing pressures. Under conditions, where CH_2Cl is maximized relative to the other products only about half of the precursor is pyrolyzed.

Following supersonic expansion, the radicals are skimmed twice before entering the reaction chamber. Experiments are carried out in the leading edge of the molecular pulse in order to take advantage of velocity slip and minimize signals from the photodissociation of CH_2ClI [2,15].

2.2. Photodissociation and detection of products

Radical photolysis and product detection are achieved using the frequency doubled output of Nd:YAG pumped dye laser systems. In the case of H-atom products, a single laser at $\lambda = 243.14$ nm is used for both photolysis and product ionization. Less than 0.1 mJ of laser energy is used in a beam focused with a 46.0 cm focal length lens. Hydrogen atoms are ionized by 2 + 1 REMPI. To interrogate $Cl(^2P_{3/2})$ products with ~243 nm photolysis, one laser system is used for photolysis (pump) and the other to ionize the product (probe). The pump laser wavelength is slightly shifted from the hydrogen atom REMPI wavelength, to $\lambda_{\text{phot}} = 243.23$ nm, in order to avoid space charge effects due to simultaneous ionization of H-atoms. $Cl(^2P_{3/2})$ products are usually ionized by 2 + 1 REMPI at $\lambda_{\text{phot}} = 235.34$ nm via the $^2D_{3/2} \leftarrow {}^2P_{3/2}$ transition [16]. The polarizations of the two lasers are fixed parallel to each other and kept perpendicular to the plane defined by the molecular beam and the laser propagation axis. Using unpolarized

probe radiation, or REMPI transitions via the $^2S_{1/2} \leftarrow {}^2P_{1/2}$ and $^2P_{1/2} \leftarrow {}^2P_{1/2}$ transitions did not lead to significant changes in the speed-dependent angular distributions, within our experimental accuracy. Thus, alignment effects are not important for assessing the contributions of the parallel and perpendicular transitions to the images. The pump (1.0 mJ) and probe (0.15 mJ) laser beams are focused with 40.0 and 30.0 cm focal length lenses, respectively. During the acquisition of an image, the probe laser is scanned over the full Doppler profile of the monitored fragment.

The velocity mapping photofragment ion imaging arrangement used for product detection has been described previously [16,17]. In brief, it consists of an ion-acceleration stage, a 60-cm long drift tube, and a CCD camera that monitors a phosphor screen coupled to a MCP detector. The ion-optics consists of a repeller, an open extractor electrode, and an open ground electrode.

2.3. Image processing

Background signals are subtracted from the images obtained in two-color pump and probe experiments. First, the signal generated by the probe laser alone is monitored. Then, the 'dark noise' of the CCD camera is collected with both the pump and probe lasers off. In the one-color experiments, the main background arises from H-ions generated from the residual gas, which have isotropic angular distributions. The signal generated with the nozzle closed is subtracted to eliminate the contribution of this background. Additionally, the signals obtained with the pyrolysis tube heating on and off are always compared in order to verify that the signal originates from the radical. The resultant images are normalized to the relative sensitivity of the pixels in the CCD camera. The inverse Abel transform is performed on the normalized signal to extract the 3D distributions [17–19].

The fragment translational energy distribution is derived from the speed distribution, which is obtained from the transformed images by integrating the signal for each radial distance from the center (after calibrating the image for conversion from distance to speed). The total center-of-mass (c.m.) translational energy distribution, E_t, is derived by scaling according to the mass ratio dictated by the momentum and energy conservation. We only display the c.m. translational energy distribution above 1900 cm^{-1}, because in the Abel transform the errors accumulate towards the center of the image, which corresponds to low translational energies (see Figs. 1 and 2).

We have discussed the determination of the angular distribution in detail previously [20]. Briefly, to obtain the speed-dependent angular distributions the velocities within a prescribed small velocity range Δv are summed and the value of the recoil anisotropy parameter, $\beta_{eff}(v)$, is determined in the usual manner [2,20,21]. The limiting values of β are +2.0 and −1.0 for parallel and perpendicular transitions, respectively. In a parallel transition in CH_2Cl, the transition dipole moment is parallel to the C–Cl bond [2].

3. Results and analysis

As discussed above, with 235–243 nm photolysis simultaneous transitions to several excited states are evident. Fig. 1a depicts an Abel transformed image of $Cl(^2P_{3/2})$ obtained with 243.23 nm photolysis. In this figure, as in all other images, the electric field vector of the photolysis laser is parallel to the vertical direction of the image plane. Fig. 1b shows the total photoproduct c.m. translational energy and the anisotropy parameter distributions obtained by monitoring $Cl(^2P_{3/2})$. The width of the $Cl(^2P_{3/2})$ translational energy distribution corresponds to a range of internal excitations in the CH_2 co-fragment, as discussed in our previous work [2]. The energy thresholds for the production of the ground and first excited states of the CH_2 co-fragment are indicated in Fig. 1b.

In our previous work we obtained the values of $\beta = 1.2 \pm 0.1$ and -0.7 ± 0.1 for the parallel and perpendicular transitions, respectively, which were *speed-independent* [2]. At $\lambda_{phot} = 243.24$ nm, β_{eff} of $Cl(^2P_{3/2})$ is different than these previous values and is speed dependent, i.e., products with higher translational energies have smaller values of β_{eff} (down to −0.4) than do those with lower translational energies (up to 0.2). The variations are re-

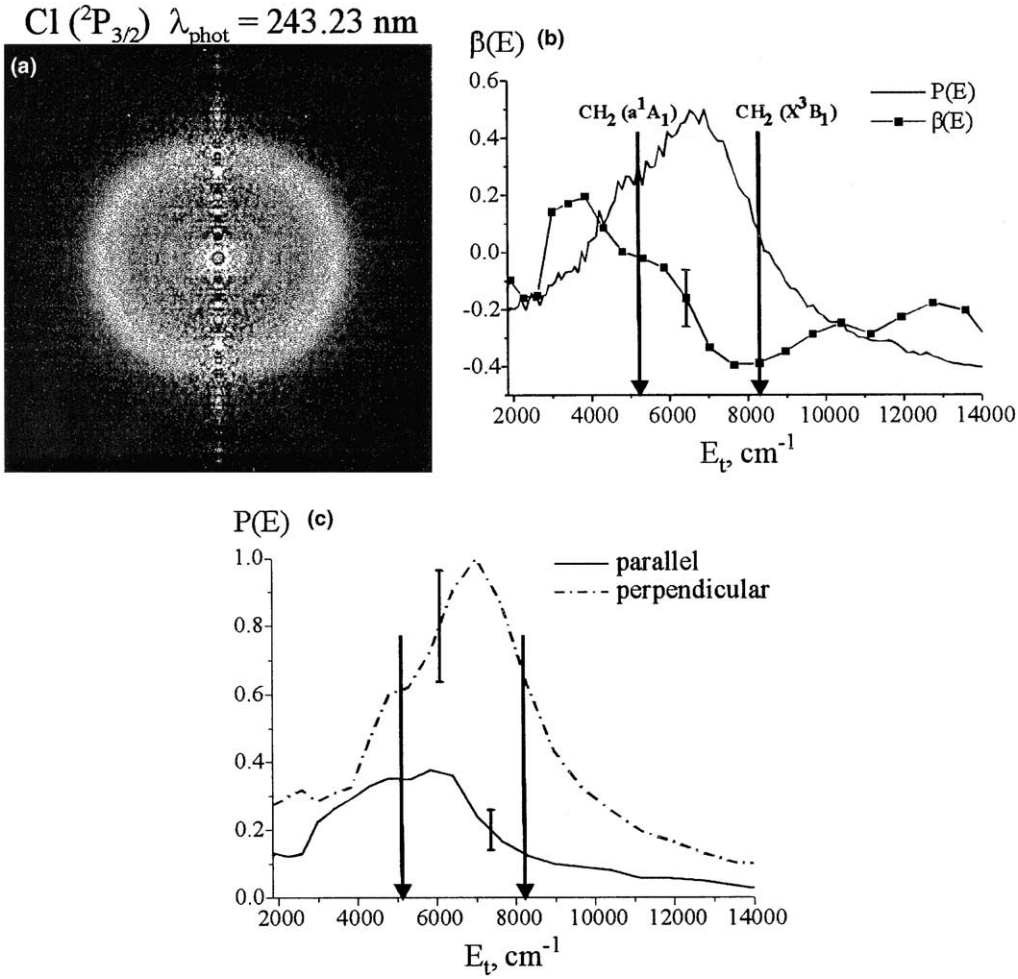

Fig. 1. (a) Abel transformed image of $Cl(^2P_{3/2})$ obtained from CH_2Cl photodissociation at 243.23 nm. $Cl(^2P_{3/2})$ is detected by $(2+1)$ REMPI at 235.34 nm. The electric field vector of the photolysis laser is parallel to the vertical direction of the image plane. (b) $Cl(^2P_{3/2})$ signals as a function of total c.m. photofragment translational energy, E_t, are given by the solid curve (arbitrary units). The squares show the values of the recoil anisotropy parameter, β_{eff}, determined at specific translational energies. The connecting lines are for convenience of viewing. The error bar depicts the typical error in the measurement of β_{eff}, and the long arrows indicate the energy thresholds for the production of $CH_2(\tilde{X}^3B_1)$ and $CH_2(\tilde{a}^1A_1)$ from vibrationally cold CH_2Cl. (c) Product c.m. translational energy distributions for the perpendicular (dot–dashed curve) and the parallel (solid curve) transitions extracted from the total c.m. translational energy distribution shown in (b) as described in the text. The plotted probabilities reflect the relative populations. The error bars are determined by the uncertainty in β_{eff}.

producible and larger than the measurement error. Our results at $\lambda_{phot} = 235.34$ nn, presented previously [2], show a similar behavior of β_{eff} as a function of speed both for $Cl(^2P_{3/2})$ and $Cl(^2P_{1/2})$, and β_{eff} ranges from about 0.9 to 0.3. The error in the anisotropy parameter measurements reflects the spread in values obtained from several images.

In Fig. 2, an image of the H atom photoproduct obtained in a one-color experiment at 243.1 nm and the corresponding c.m. translational energy and anisotropy parameter distributions are shown. The channel II threshold is also marked. Because of high contributions from background hydrogen ions, the signal to noise ratio was poor and we

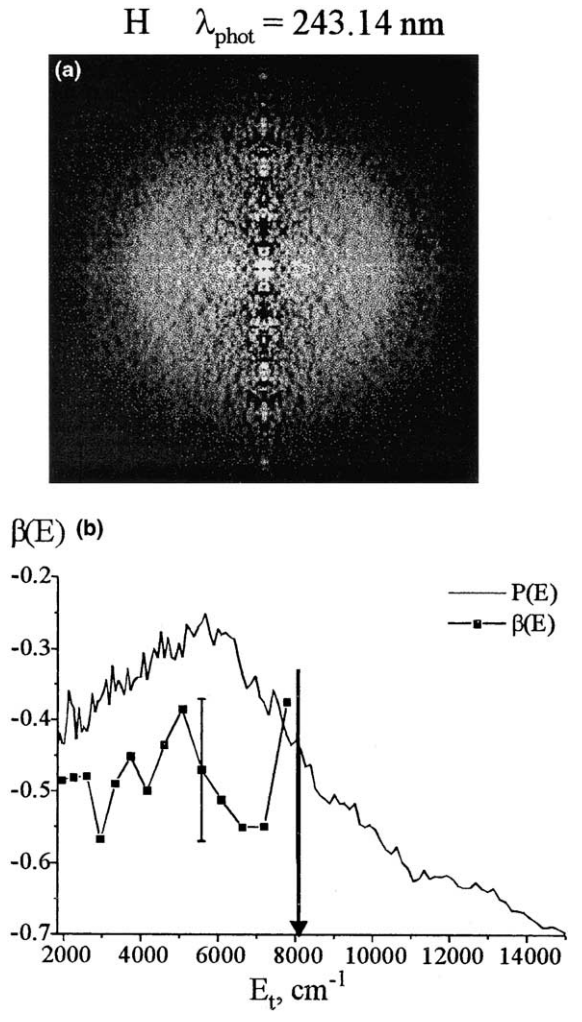

Fig. 2. (a) Abel transformed image of the H-atom photofragment obtained in a one-color experiment at 243.14 nm. The electric field vector of the photolysis laser is parallel to the vertical direction of the image plane. (b) H-atom signals as a function of the total c.m. photofragment translational energy, E_t, are given by the solid curve (arbitrary units). The squares show the values of the recoil anisotropy parameter, β_{eff}, determined at specific translational energies. The connecting lines are for convenience of viewing. The arrow indicates the energy threshold for channel II.

were able to get reliable results only for the one-color experiment. Unlike $Cl(^2P_{3/2})$ at this wavelength, the angular distribution of H is characteristic of a perpendicular electronic transition at all speeds ($\beta_{eff} = -0.5 \pm 0.1$). At translational energies greater than 8000 cm^{-1}, the anisotropy measurements become less reliable because of larger contributions from the residual H background signal, which is isotropic.

3.1. Analysis of Cl images in the region of 235–243 nm

The separate product c.m. speed distributions for the perpendicular and parallel transitions at 235–243 nm can be extracted for channel I at each dissociation wavelength from the measured speed distribution, $P(v)$, and the values of β_{eff} at each product speed v. The following assumptions are used in the extraction procedure: (i) each measured product speed distribution, $P(v)$, is a combination of two distributions, $P_1(v)$ and $P_2(v)$, which arise from the excitation of a perpendicular and a parallel transition, respectively; (ii) each of these two separate distributions is characterized by a value of the anisotropy parameter ($\beta_{1,2}$) which is speed-independent; (iii) the β values measured in photolysis regions where a single excited state is accessed can be used for the perpendicular and parallel transitions, respectively [2]. The values $\beta_1 = -0.7 \pm 0.1$ and $\beta_2 = 1.2 \pm 0.1$ were obtained for the pure perpendicular and parallel transitions excited in the regions 312–247 and 219.5–214 nm, respectively [2]. From these assumptions it follows that for each product speed v:

$$P(v) = P_1(v) + P_2(v), \tag{1}$$

$$\beta_{eff}(v) = \frac{\beta_1 P_1(v) + \beta_2 P_2(v)}{P(v)} \tag{2}$$

and, therefore,

$$P_1(v) = \frac{\beta_{eff}(V) - \beta}{\beta_1 - \beta_2} P(v), \tag{3}$$

$$P_2(v) = \frac{\beta_1 - \beta_{eff}(V)}{\beta_1 - \beta_2} P(v). \tag{4}$$

In Fig. 1c we show the separate c.m. translational energy distributions associated with the parallel and perpendicular transitions at 243.23 nm obtained by using Eqs. (3) and (4), and $\beta_2 = 1.2$ and $\beta_1 = -0.7$. The error bars shown in the figure reflect the signal to noise ratio in the measured c.m. translational energy distribution shown in Fig. 1b,

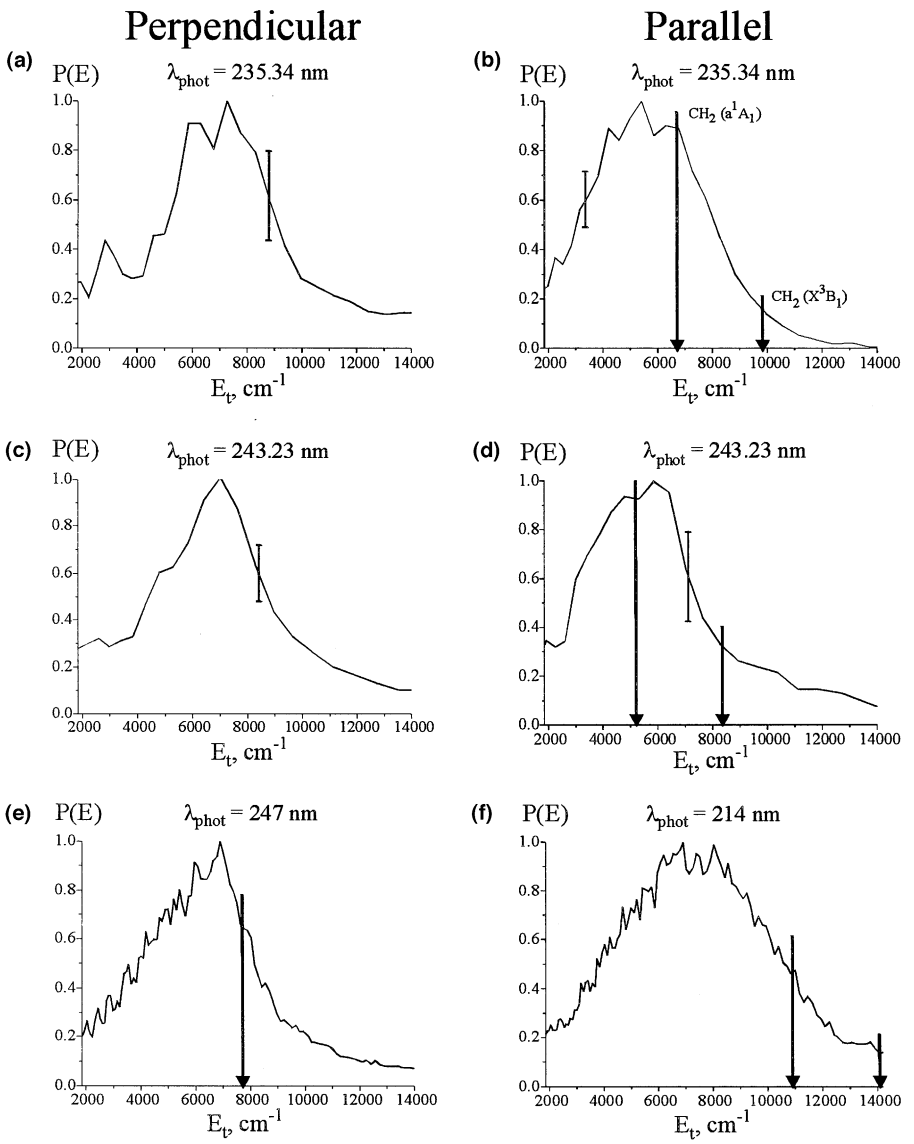

Fig. 3. In the left and right panels, the c.m. translational energy distributions for channel I ($Cl(^2P_{3/2})$ fragment) arising from the perpendicular and parallel transitions, respectively, are shown, normalized to the same maximum. At 235.34 and 243.23 nm, they are extracted from the corresponding total c.m. translational energy distributions as described in the text. In panels (e) and (f), the distributions obtained before at wavelengths where only the perpendicular or parallel transition is excited, respectively, are shown for comparison [2]. The arrow in panel (e) marks the thermochemical threshold of channel I for cold CH_2Cl radicals.

as well as the error in the measured $\beta_{\text{eff}}(v)$ values (± 0.1).

Fig. 3 shows the total c.m. translational energy distributions for the perpendicular (left panels) and parallel (right panels) transitions that were extracted from the corresponding $Cl(^2P_{3/2})$ product speed distributions obtained at $\lambda_{\text{phot}} = 235.34$ nm (panels a, b), and $\lambda_{\text{phot}} = 243.23$ nm (panels c, d). The distributions for pure perpendicular (panel e) and parallel (panel f) transitions were measured before at $\lambda_{\text{phot}} = 247$ and 214 nm, respectively [2]. Each distribution is normalized to

Table 1
Relative contributions of the perpendicular and parallel transitions

	$Cl(^2P_{3/2})$ $\lambda_{phot} = 243.23$ nm ($E_{avl} = 8430$ cm^{-1})	$Cl(^2P_{3/2})$ $\lambda_{phot} = 235.34$ nm ($E_{avl} = 9812$ cm^{-1})	$Cl(^2P_{1/2})$ $\lambda_{phot} = 235.21$ nm ($E_{avl} = 8954$ cm^{-1})
Relative yield (perpendicular/parallel)	2.6 ± 0.4	0.48 ± 0.08	0.51 ± 0.08

its maximum. We also extracted the contributions from the perpendicular and parallel transitions by monitoring $Cl(^2P_{1/2})$ at $\lambda_{phot} = 235.21$ nm (see [2, Fig. 7]). They are similar to those for $Cl(^2P_{3/2})$ at 235.34 nm.

Table 1 lists the relative contributions of the perpendicular and parallel transitions calculated by integrating the extracted perpendicular and parallel components over all speeds. As expected, the relative amount of the perpendicular component decreases with increasing excitation energy. The accuracy of the relative yield calculations reflects mainly the accuracy of determining the anisotropy parameters $\beta_{1,2}$; i.e. ± 0.1. Changing the values of $\beta_{1,2}$ within these limits does not significantly affect the shapes of the distributions, but only the relative populations.

4. Discussion

The results and analysis reported above enable us to extract the fractions of Cl products produced via either the parallel or perpendicular transitions, and determine the corresponding translational energy distributions. The main assumption involved in the analysis is that the β parameter associated with each transition does not vary with wavelength. This is a reasonable assumption, considering that all the investigated wavelengths are thousands of wave numbers above the thermochemical threshold of channel I, and the dynamical behavior appears to be dominated by strong repulsive forces. Before comparing the extracted distributions with those obtained in regions where absorption to a single electronic state dominates, the relevant excited electronic states are briefly discussed.

In recent ab initio calculations it was found that in the 300–200 nm region, three electronic transitions are allowed [3]. The two lowest-energy transitions are perpendicular; the first involves the 1^2A_1 valence state arising from $\sigma^*_{CCl} \leftarrow \pi^*_{CCl}$ excitation, and the next one excites the 2^2A_1 Rydberg state ($3s \leftarrow \pi^*_{CCl}$). Their vertical maxima are at 4.92 eV (252 nm) and 5.54 eV (224 nm), respectively. The third and strongest allowed transition, whose calculated vertical maximum is at 6.33 eV (196 nm), is parallel and involves excitation to the valence 2^2B_1 state ($\pi^*_{CCl} \leftarrow \pi_{CCl}$). Because excitation to the two valence states involves promoting an electron to a C–Cl antibonding orbital, it is not surprising that Cl is the dominant dissociation product.

A distinctive feature of the perpendicular transition giving rise to channel I is the intense 'hot band' absorption observed even in the supersonic beam. At wavelengths >260 nm and with He as a carrier gas, at least half of the Cl products are generated via hot band excitation, and although this fraction diminishes at higher excitation energies, it is still significant at 247 nm. Previously, we identified the C–Cl stretch as a major contributor to the hot bands, and concluded that the C–Cl bond length in the ground and 1^2A_1 states must be quite different [2]. It is likely that the 1^2A1 state is bound in the C–Cl coordinate, but that at the wavelengths where absorption is significant, the radical is excited to regions of the potential energy surface that are repulsive in the C–Cl coordinate. The Cl translational energy distributions obtained from images taken at $\lambda_{phot} < 266$ nm indicate that a large fraction of the available energy is deposited in relative translation. $CH_2(\tilde{X}^3B_1)$ and $Cl(^2P_{3/2})$ are the main photofragments.

The parallel transition observed at $\lambda_{phot} =$ 214–220 nm is at the red wing of the strong transition whose observed peak is around 200 nm [2,4]. We find that $Cl(^2P_{3/2})$ and $Cl(^2P_{1/2})$ are produced in comparable amounts at these wavelengths, and $CH_2(\tilde{a}^1A_1)$ appears to be the predominant state of

the methylene co-fragment. The Cl translational energy distributions are broad and their maxima are at energies where about half the available energy is deposited as internal energy (electronic, vibrational and rotational) of the methylene co-fragment. The excited $^2B_1$ state is probably repulsive [2].

The photolysis wavelengths used in the present work correspond to the red wing of the parallel transition and the blue wing of the valence perpendicular transition. Inspection of the extracted Cl distributions for the perpendicular transition shows that, in accordance with the trends observed before, the distributions contain a diminishing fraction from 'hot band' excitation at the shorter wavelengths, and most of the fragments have high translational energies. However, we find that although in the peak region of the transition, $Cl(^2P_{3/2})$ is the dominant product, $Cl(^2P_{1/2})$ images obtained at 235.21 nm and 240.25 nm (not shown here), although exhibiting overall a positive β_{eff}, contain a significant fraction of $Cl(^2P_{1/2})$ products that derives from the perpendicular transition. Not surprisingly, the exit-channel interactions that are responsible for mixing the two spin-orbit states of chlorine depend on the excitation energy.

As expected, at shorter wavelengths the fraction of the parallel transition increases relative to the contribution from the perpendicular transition. The translational energy distribution of the parallel Cl component resembles qualitatively the distributions obtained in regions where this transition dominates [2]; i.e. hot-bands are less important than in the perpendicular transition, and the translational energy distributions correspond to a large fraction of the available energy in the internal degrees of freedom of the CH_2 co-fragment. From the measurements at 220–214 nm we concluded that $CH_2(\tilde{a}^1A_1)$ is the main product [2]. At the lower excitation energies studied here, we find that a larger fraction of the products have internal energies that are lower than the excitation energy necessary to reach the $CH_2(\tilde{a}^1A_1)$ state (at 3147 cm^{-1}). It appears therefore that the fraction of ground-state methylene increases at lower excitation energies. Extrapolating from the measured shape of the CH_2Cl absorption spectrum in the region of the parallel transition [4], we estimate that the absorption cross section at 235–243 nm is more than an order of magnitude lower than the absorption at the peak.

In contrast to the Cl angular distribution obtained at 243.24 nm, the H-photofragment at 243.14 nm arises exclusively from *perpendicular* transition(s), and the measured value of $\beta_{eff} = -0.5 \pm 0.1$ is speed independent. The H-photofragment energy distribution is quite different from the corresponding perpendicular component of the Cl distribution at the same photolysis wavelength. Although both the Cl and H translational energy distributions exhibit a larger hot band component than do the Cl distributions from the parallel transition, a smaller fraction of the available energy appears as translational energy for channel II than it does for channel I. Furthermore, the c.m. translational energy distribution of channel II is rather similar to the one observed in the $CH_3 \rightarrow H + CH_2$ dissociation from the 3s Rydberg state [1]. North et al. obtained a negative β parameter for this process at 193.3 nm, and determined that the c.m. translational energy distribution is broad and peaks at ~ 5000 cm^{-1}, while the total available energy is $\sim 12\,200$ cm^{-1}. In our case, the translational energy distribution for channel II is broad as well, and extends down to the lowest translational energies. Since the vertical maximum of the $3s \leftarrow 1^2B_1$ transition is calculated to lie at $\sim$224 nm [3], excitation at 243 nm would be at the red wing of this transition (whose adiabatic origin is yet unknown), and might also contribute to the observed signal. A study of the H-photofragment yield spectrum and its comparison to the Cl photofragment yield spectrum should shed further light on the nature of the participating states, but unfortunately could not be carried out with our present experimental arrangement because of the small signals and the large H-background discussed above.

In summary, the Cl images in the spectral region 235–243 nm indicate that both the perpendicular ($1^2A_1 \leftarrow 1^2B_1$) and parallel ($2^2B_1 \leftarrow 1^2B_1$) transitions contribute significantly to Cl formation via channel I, with the fraction of the parallel transition increasing as the wavelength is decreased. The shapes of the translational energy distributions, which are determined by the shape of the potential energy surface near the Franck–Condon region for

excitation, remain qualitatively similar to those obtained in regions where the transitions are isolated. The fractions of the electronic and spin-orbit states of the products, which depend on specific surface crossings, change with excitation wavelength. H-atom is identified as a minor product. We raise the possibility that in addition to the $1^2A_1 \leftarrow 1^2B_1$ perpendicular transition, excitation to the Rydberg 3s state also contributes to H-formation. Although we do not have a direct proof for the participation of the Rydberg state, nor do we know the corresponding band origin of the transition, the H-atom distributions (angular and energy) are qualitatively similar to those obtained in the dissociation of the methyl radical from the 3s state at 193.3 nm [1,3]. Therefore, this suggestion merits further investigation.

Acknowledgements

This work was supported by the National Science Foundation and the Donors of the Petroleum Research Fund, administered by the American Chemical Society is gratefully acknowledged. We benefited greatly from discussions with Anna Krylov, Sergei Levchenko and Pavel Jungwirth.

References

[1] S.W. North, D.A. Blank, P.M. Chu, Y.T. Lee, J. Chem. Phys. 102 (1995) 792.
[2] V. Dribinski, A.B. Potter, A.V. Demyanenko, H. Reisler, J. Chem. Phys. 115 (2001) 7474.
[3] S.V. Levchenko, A.I. Krylov, J. Chem. Phys. 115 (2001) 7485.
[4] P.B. Roussel, P.D. Lightfoot, F. Caralp, V. Catoire, R. Lesclaux, W. Forst, J. Chem. Soc. Faraday Trans. 87 (1991) 2367.
[5] S.G. Lias, J.E. Bartmess, J.F. Liebman, J.L. Holmes, R.D. Levin, W.G. Mallard, J. Phys. Chem. Ref. Data 17 (1988).
[6] NIST Chemistry WebBook: NIST Standard Reference Database No. 69 (February 2000 Release); http://webbook.nist.gov/chemistry.
[7] J.J. DeCorpo, D.A. Bafus, J.L. Franklin, J. Chem. Thermodyn. 3 (1971) 125.
[8] M. Weissman, S.W. Benson, J. Phys. Chem. 87 (1983) 243.
[9] E. Tschuikow-Roux, S. Paddison, Int. J. Chem. Kinet. 19 (1987) 15.
[10] J.L. Holmes, F.P. Lossing, J. Am. Chem. Soc. 110 (1988) 7343.
[11] J.A. Seetula, J. Chem. Soc. Faraday Trans. 92 (1996) 3069.
[12] J.A. Seetula, Phys. Chem. Chem. Phys. 2 (2000) 3807.
[13] D.W. Kohn, H. Clauberg, P. Chen, Rev. Sci. Instrum. 63 (1992) 4003.
[14] S.A. Wright, J.D. McDonald, J. Chem. Phys. 101 (1994) 238.
[15] E. Kolodney, A. Amirav, Chem. Phys. 82 (1983) 269.
[16] S. Arepalli, N. Presser, D. Robie, R.J. Gordon, Chem. Phys. Lett. 118 (1985) 88.
[17] Th. Droz-Georget, M. Zyrianov, H. Reisler, D. Chandler, Chem. Phys. Lett. 276 (1997) 316.
[18] M. Zyrianov, A. Sanov, Th. Droz-Georget, H. Reisler, J. Chem. Phys. 110 (1999) 10774.
[19] R.N. Bracewell, The Fourier Transform and its Applications, McGraw-Hill, New York, 1986.
[20] A.V. Demyanenko, V. Dribinski, H. Reisler, H. Meyer, C.X.W. Qian, J. Chem. Phys. 111 (1999) 7383.
[21] A.J.R. Heck, D.W. Chandler, Annu. Rev. Phys. Chem. 46 (1995) 335.